

1 **E4 LIGASE SPECIFIC UBIQUITYLATION HUBS**  
2 **COORDINATE DNA DOUBLE STRAND BREAK REPAIR**  
3 **AND APOPTOSIS**

4 **Leena Ackermann<sup>1,5</sup>, Michael Schell<sup>1,5</sup>, Wojciech Pokrzywa<sup>1</sup>, Éva Kevei<sup>1</sup>, Anton**  
5 **Gartner<sup>2</sup>, Björn Schumacher<sup>3,4,\*</sup> & Thorsten Hoppe<sup>1,\*</sup>**

6

7 <sup>1</sup>Institute for Genetics and CECAD Research Center  
8 University of Cologne  
9 Cologne, Germany

10  
11 <sup>2</sup>Centre for Gene Regulation and Expression  
12 School of Life Sciences  
13 University of Dundee  
14 Scotland

15  
16 <sup>3</sup>Institute for Genome Stability in Aging and Disease  
17 Medical Faculty  
18 University of Cologne  
19 Cologne, Germany

20  
21 <sup>4</sup>CECAD Research Center and Center for Molecular Medicine Cologne  
22 University of Cologne  
23 Cologne, Germany

24  
25 <sup>5</sup>These authors contributed equally to this work

26  
27

28 \*Correspondence should be addressed to B.S. or T.H.

29 \*Correspondence: [bjorn.schumacher@uni-koeln.de](mailto:bjorn.schumacher@uni-koeln.de)

30 Phone: +49 221 478 84202

31 Fax: +49 221 478 84204

32

33 [thorsten.hoppe@uni-koeln.de](mailto:thorsten.hoppe@uni-koeln.de)

34 Phone: +49 221 478 84218

35 Fax: +49 221 478 84217

36

37 **Multiple protein ubiquitylation events at DNA double strand breaks (DSBs) regulate**  
38 **damage recognition, signaling and repair. It has remained poorly understood how the**  
39 **repair process of DSBs is coordinated with the apoptotic response. Here, we identified**  
40 **the E4 ubiquitin ligase UFD-2 as a mediator of DNA damage-induced apoptosis in a**  
41 **genetic screen in *Caenorhabditis elegans*. We demonstrate that upon initiation of**  
42 **homologous recombination by RAD-51, UFD-2 forms foci that contain substrate**  
43 **processivity factors including the ubiquitin-selective segregase CDC-48(p97), the**  
44 **deubiquitylation enzyme ATX-3(Ataxin-3), and the proteasome. In the absence of UFD-**  
45 **2, RAD-51 foci persist and DNA damage-induced apoptosis is prevented. In contrast,**  
46 **UFD-2 foci are retained until recombination intermediates are removed by the Holliday**  
47 **junction processing enzymes GEN-1, MUS-81 or XPF-1. UFD-2 foci formation also**  
48 **requires pro-apoptotic CEP-1(p53) signaling. Our findings establish a central role for**  
49 **UFD-2 in the coordination between the DNA repair process and the apoptotic response.**

50

## 51 **INTRODUCTION**

52 DNA double strand breaks (DSBs) are highly cytotoxic and require the assembly of DNA  
53 damage signaling complexes and the DSB repair machinery at the DNA breaks <sup>1</sup>. In the *C.*  
54 *elegans* germline DSBs are mainly repaired by homologous recombination (HR) <sup>2</sup>. After  
55 initial processing of the damaged site, RAD-51 accumulates on single stranded DNA  
56 (ssDNA) overhangs and mediates strand invasion into the undamaged template, thus  
57 facilitating recombination and repair. Ultimately cruciform recombination intermediates  
58 called Holliday junctions (HJ) are formed <sup>3</sup>. HJs can be processed by two major pathways: HJ  
59 dissolution via the combined action of the Bloom's syndrome helicase and Topoisomerase  
60 TopoIII $\alpha$  <sup>4</sup>, or by resolution of HJs by nucleases acting as resolving enzymes <sup>5</sup>. While HJ  
61 dissolution predominates in most systems <sup>6,7</sup>, in *C. elegans* the GEN-1 resolvase is needed for

62 completion of HR repair of DSBs<sup>8</sup>. The resolution of HR intermediates is important for the  
63 apoptotic response to DSBs as GEN-1 and HJ processing factors are required for DNA  
64 damage-induced programmed cell death. While the mechanisms for such regulation are not  
65 known yet, the C-terminal non-catalytic domain of GEN-1 appears to be important for DNA  
66 damage signaling<sup>8,9</sup>. The apoptotic response to persistent DSBs facilitates the removal of  
67 germ cells in *C. elegans* when DSBs or meiotic recombination intermediates are not repaired,  
68 and occurs in the meiotic pachytene zone of the nematode germline<sup>10</sup>. DNA damage  
69 checkpoint signaling leads to the activation of the *C. elegans* p53 homolog CEP-1 followed  
70 by the induction of apoptosis<sup>11,12</sup>. CEP-1/p53 protein becomes available in the late pachytene  
71 region of the germline, leading to apoptosis competency of these germ cells. CEP-1  
72 expression in earlier stages of meiosis is translationally repressed by the conserved mRNA  
73 binding protein GLD-1<sup>13</sup>. Thus, apoptosis is only initiated when aberrant meiotic  
74 recombination intermediates or ionizing radiation (IR)-induced DSBs persist in late pachytene  
75 cells. It remains, however, unclear how DNA damage processing by recombination repair is  
76 coordinated with the apoptosis pathway to allow sufficient time to resolve HR intermediates.

77 In order to better understand how the apoptotic response to DSBs is regulated, we undertook a  
78 genetic screen in *C. elegans* for defects in the IR-induced germ cell apoptosis. RNAi  
79 knockdown and genetic mutation of *ufd-2* resulted in a reduced apoptotic response. We  
80 demonstrate that upon initiation of HR by the recombinase RAD-51, UFD-2 forms foci that  
81 we define as ubiquitylation hubs as they also contain substrate CDC-48, ATX-3, and the  
82 proteasome. In the absence of UFD-2 or its catalytic activity, RAD-51 foci persist. Similarly  
83 to *ufd-2* deficiency, elevated RAD-51 levels result in reduced apoptosis. When the resolution  
84 of HJs is hampered due to the absence of GEN-1, MUS-81, or XPF-1, UFD-2 foci persist.  
85 UFD-2 foci formation not only requires RAD-51 but also pro-apoptotic signaling through the  
86 *C. elegans* p53 homolog CEP-1. We thus propose that UFD-2 specific ubiquitylation hubs

87 link pro-apoptotic and DNA repair signaling to coordinate the apoptotic response with  
88 ongoing DSB repair activity.

89

## 90 **RESULTS**

### 91 **Ligase activity of UFD-2 triggers DSB-induced apoptosis**

92 To identify new regulators of the apoptotic response to DNA damage, we performed an RNA  
93 interference (RNAi) screen targeting 770 genes whose transcription is enriched in the *C.*  
94 *elegans* germline<sup>14</sup> (**Fig. 1a**). We focused on those candidate genes because in *C. elegans*  
95 DNA damage induced apoptosis only occurs in germ cells<sup>10,15</sup>. We identified the E4 ubiquitin  
96 ligase UFD-2 as the most prominent hit resulting from our screen. RNAi against *ufd-2* led to a  
97 dose dependent reduction of IR induced apoptosis (**Fig. 1b**), a phenotype confirmed by  
98 analyzing the two different null alleles *ufd-2(tm1380)* and *ufd-2(hh1)* (**Fig. 1c, d**). In contrast,  
99 neither developmental apoptosis that occurs during the somatic development of the worm, nor  
100 physiological germ cell apoptosis, a background level of germ cell apoptosis that occurs  
101 independently of DNA damage, was defective in *ufd-2* mutants (**Supplementary Fig. 1a, b**).

102 UFD-2 participates in the ubiquitin fusion degradation (UFD) pathway that was first  
103 identified in budding yeast<sup>16</sup>. Substrate ubiquitylation involves E1 ubiquitin activating, E2  
104 ubiquitin conjugating, and E3 ubiquitin ligase enzymes. UFD-2 defines a class of so-called E4  
105 enzymes, which further elongate pre-existing ubiquitin chains to facilitate efficient  
106 proteasomal degradation<sup>17-20</sup>. It preferentially targets lysine residues 29 and 48 of ubiquitin  
107 for autoubiquitylation (**Supplementary Fig. 1e**). A P951A point mutation in the U-box  
108 domain completely blocks the ligase activity of UFD-2<sup>21</sup> (**Fig. 1e**). To determine if UFD-2  
109 catalytic activity was required for DNA damage-induced apoptosis, we transgenically  
110 expressed UFD-2::GFP or UFD-2<sup>P951A</sup>::GFP in the germline of wild-type or the *ufd-2* deletion

111 background. Importantly, UFD-2::GFP expression fully restored the apoptotic DNA damage  
112 response in *ufd-2(tm1380)* mutant animals (**Fig. 1f**). In contrast, the catalytically dead mutant  
113 UFD-2<sup>P951A</sup>::GFP showed strongly reduced apoptosis after treatment with 60 Gy IR  
114 comparable to *ufd-2* deletion mutant. Overexpression of UFD-2<sup>P951A</sup>::GFP in the wild-type  
115 background also caused defective apoptosis, which indicates that the inactive U-box mutant  
116 acts dominant-negatively in response to DNA damage (**Fig. 1f**).

117

### 118 **UFD-2 forms focal accumulations upon DSB induction**

119 To determine *in vivo* localization, we raised polyclonal antibodies that specifically recognize  
120 UFD-2 both by western blot analysis and immunofluorescence staining (**Fig. 2a and**  
121 **Supplementary Fig. 2a**). Using immunostaining, we found that under unperturbed conditions  
122 the protein was evenly distributed in the *C. elegans* germ line syncytium (**Supplementary**  
123 **Fig. 2b**). Commencing from late pachytene cells, UFD-2 accumulated at the nuclear periphery  
124 resulting in a ring-shaped staining pattern. After IR treatment, UFD-2 foci of varying size and  
125 number became detectable within the nucleoli (**Fig. 2a, b and Supplementary Fig. 2b**). The  
126 pattern of antibody staining was confirmed by GFP-tagged UFD-2 transgenes (**Fig. 2c, d**).  
127 These UFD-2 foci occurred in the mitotic zone (data not shown) as well as in the mid-late  
128 pachytene zone of the germline after IR (**Supplementary Fig 2b**). Given our interest in  
129 apoptosis we focused on UFD-2 foci formation in the pachytene region. Pachytene cells elicit  
130 DNA damage-induced apoptosis upon DNA damage checkpoint activation, whereas mitotic  
131 nuclei in the distal germ line compartment are subjected to cell cycle arrest<sup>10</sup>. In contrast to  
132 the IR-induced apoptosis defect, the cell cycle arrest, which can be monitored by scoring the  
133 number of mitotic nuclei that are enlarged due to continuous growth of cellular and nuclear  
134 compartments in the absence of cell division (**Supplementary Fig. 1c, d**)<sup>10,22</sup>, was normally  
135 induced in *ufd-2* mutant animals, suggesting that the DNA damage checkpoint in general was

136 functional. Unlike IR-induced RAD-51 repair foci, which accumulate immediately upon  
137 damage induction, UFD-2 foci were not yet detectable 5 hrs following damage  
138 **(Supplementary Fig. 2c, d)**. We therefore scored UFD-2 foci formation 24 hrs after IR, a  
139 time concurrent with full apoptosis activation <sup>10</sup>, using both antibodies and GFP transgenes.  
140 The number of foci observed in pachytene cells increased from 0-5 foci per germline to more  
141 than 15 upon treatment with 60 Gy of IR **(Fig. 2a-d and Supplementary Fig. 2b, c)**.  
142 Surprisingly, the ubiquitin ligase mutant was equally efficient in UFD-2 foci formation as the  
143 wild-type ligase **(Fig. 2 c, d)**. Together, these data indicate that the UFD-2 ligase activity is  
144 required to trigger DNA damage-induced apoptosis **(Fig. 1f)**, but is not necessary for UFD-2  
145 foci formation **(Fig. 2c, d)**.

146

#### 147 **Ubiquitin signaling fine-tunes the apoptotic response**

148 Given that UFD-2 triggers protein degradation <sup>16,17,23</sup>, we examined if factors associated with  
149 the ubiquitin-proteasome system (UPS) might associate with UFD-2 foci <sup>17,24,25</sup>. Hence, we  
150 analyzed ubiquitin localization 24 hrs after irradiation. In fact, an antibody recognizing  
151 conjugated mono- and polyubiquitin chains co-stained UFD-2 foci **(Fig. 3a and**  
152 **Supplementary Fig. 3e)**. Additional staining experiments detected co-localization of the  
153 proteasome and the ubiquitin-selective segregase CDC-48 with UFD-2 foci **(Fig. 3a)**. Among  
154 other processes, CDC-48/p97 has been established to coordinate the degradation of  
155 chromatin-associated proteins during DNA replication or DNA repair by extracting  
156 ubiquitylated substrate proteins from higher order complexes <sup>26-28</sup>. As CDC-48 has been  
157 shown to interact with UFD-2 <sup>20</sup>, we wondered if the interaction was necessary for UFD-2  
158 dependent apoptotic signaling. Transgenic overexpression of UFD-2<sup>C448Y</sup>::GFP, a mutant  
159 version that provides ligase activity but is not able to interact with CDC-48 <sup>29</sup>, led to UFD-2  
160 foci even without IR treatment **(Supplementary Fig. 3f-j)**. However, UFD-2<sup>C448Y</sup>::GFP failed

161 to rescue the apoptosis phenotype displayed by *ufd-2* deletion worms (**Fig. 3g**), suggesting  
162 that in addition to ligase activity also the interaction with CDC-48 is a prerequisite for the  
163 apoptotic function of UFD-2. CDC-48 has been demonstrated to guide ubiquitin chain  
164 topology by coordinating different substrate processing enzymes such as UFD-2 and the  
165 deubiquitylation enzyme ATX-3<sup>20</sup>. Intriguingly, we also found that ATX-3 localized to UFD-  
166 2 foci (**Fig. 3a and Supplementary Fig. 3c, d**), which indicates an orchestrated action of  
167 UFD-2, ATX-3, and CDC-48 at ubiquitylation hubs triggered by DNA damage. The  
168 ubiquitylation activity of UFD-2 was dispensable for the recruitment of the proteasome, ATX-  
169 3, and CDC-48 (**Fig. 3b**). In contrast, apoptosis induction required the catalytic activity of  
170 UFD-2 as well as its interaction with CDC-48 (**Fig. 1e, f, and 3g**).

171         Given that in yeast and humans, Ufd2/UBE4B mediates elongation of preformed  
172 ubiquitin chains, we tested whether UFD-2 cooperates with the E3 ligase HECD-1, the  
173 ortholog of budding yeast Ufd4 and human HECTD1 or TRIP12, to trigger DNA damage  
174 induced apoptosis<sup>17,30-32</sup>. Indeed, loss of HECD-1 prevented UFD-2 foci formation,  
175 suggesting ubiquitin-dependent recruitment of UFD-2 (**Fig. 3c, d**). Apoptosis was reduced in  
176 *hecd-1* mutants, which implicates a role of UFD-2 focal accumulation in response to DNA  
177 damage (**Fig. 3e**). The apoptosis defect was even more pronounced in *ufd-2; hecd-1* double  
178 mutants, indicating that the activity of both enzymes is required to achieve apoptosis (**Fig.**  
179 **3e**). In contrast, the deubiquitylation enzyme ATX-3 counteracted UFD-2 recruitment as both  
180 UFD-2 foci formation and apoptosis were increased in *atx-3* mutants (**Fig. 3c, d, f**).  
181 Accordingly, the excessive DNA damage-induced apoptosis occurring in *atx-3* mutants was  
182 suppressed in *ufd-2; atx-3* double mutant worms (**Fig. 3f**). The number of ubiquitin foci per  
183 germline was decreased in *hecd-1*, whereas it was increased in *atx-3* (**Fig. 3c, d and**  
184 **Supplementary Fig. 3k**). This observation suggests ubiquitin dependent formation of UFD-2  
185 foci, determined by ubiquitin-mediated recruitment signals fine-tuned by HECD-1 and ATX-

186 3. We therefore conclude that the apoptotic response to DNA damage is coordinated by  
187 ubiquitylation signals defined by UFD-2 in cooperation with HECD-1 and ATX-3.

188

### 189 **UFD-2 supports RAD-51 dissociation from DNA repair sites**

190 Next we analyzed if UFD-2 also affects the DNA repair process in addition to apoptosis. In  
191 contrast to DSB induction by IR, UV irradiation did not result in formation of UFD-2 foci  
192 consistent with a specific role of UFD-2 in responding to DSBs (**Supplementary Fig. 3a**). In  
193 line with this observation, we found that RPA-1::GFP and BRD-1::GFP HR fusion proteins  
194 <sup>33,34</sup> accumulate in UFD-2 foci 24 hrs after IR treatment (**Fig. 4a, b**). Furthermore, IR of L4  
195 staged *ufd-2* mutant larvae resulted in reduced embryonic survival in the ensuing generation  
196 (**Supplementary Fig. 3b**). To establish whether *ufd-2* promotes the processing of DNA repair  
197 intermediates, we analyzed the kinetics of RAD-51 foci. While both wild-type and *ufd-2*  
198 mutants accumulated an equal amount of RAD-51 positive nuclei one hour after IR, twice as  
199 many RAD-51 stained nuclei persisted 16 hrs later in *ufd-2* mutants (**Fig. 4c, d**). This delay in  
200 RAD-51 foci dissociation that temporally coincides with UFD-2 foci formation suggests that  
201 UFD-2 contributes to resolution of repair intermediates.

202

### 203 **UFD-2 acts downstream of pro-apoptotic signaling**

204 We next wished to further investigate the role of the DSB repair process in UFD-2 foci  
205 formation (**Fig. 4a**). Impairment of HR in *rad-51* deletion mutant worms blocked UFD-2 foci  
206 formation (**Fig. 5b**). Conversely, *rad-54* deletion defective in removal of RAD-51 from DNA  
207 during HR repair <sup>35</sup> caused an accumulation of UFD-2 foci (**Fig. 5b**). The nucleases GEN-1,  
208 MUS-81 and XPF-1 are required for the resolution of HJs in order to complete the HR repair  
209 process of IR-induced DSBs <sup>8,36,37</sup>. Deletion of the *gen-1*, *mus-81*, and/or *xpf-1* HJ processing  
210 enzymes also led to focal accumulation of UFD-2 (**Fig. 5c and Supplementary Fig. 4a**). Of



211 note, *mus-81* and *xpf-1* mutant animals showed elevated numbers of UFD-2 foci also in the  
212 absence of IR-induced DSBs consistent with the function of MUS-81/XPF-1 in meiotic HJ  
213 resolution<sup>36,37</sup>. These results indicate that HR needs to commence for UFD-2 foci to form,  
214 which persist until HR is completed (**Fig. 5b, c**).

215 As *ufd-2* mutant worms displayed reduced apoptosis, we assessed whether apoptotic  
216 signaling was affected in *ufd-2* mutant worms. The apoptotic core machinery is conserved  
217 from *C. elegans* to the mammalian system. The p53 homologue CEP-1 induces transcription  
218 of the two BH3-only proteins EGL-1 and CED-13<sup>13,38</sup>, which bind to the only Bcl2-like  
219 protein CED-9. As a consequence, the inhibitory effect of CED-9 on the Apaf1-like CED-4 is  
220 alleviated and CED-4 activates the caspase CED-3, which executes cell death (**Fig. 5a**)<sup>39</sup>. In  
221 view of the ubiquitin ligase activity, we tested whether CEP-1 protein might accumulate upon  
222 DNA damage in the absence of UFD-2. However, in wild-type and *ufd-2* mutant worms CEP-  
223 1 protein was equally expressed following 60 Gy irradiation (**Supplementary Fig. 4b-d**).  
224 Additional evaluation of mRNA transcripts of the CEP-1 target gene *egl-1* showed a  
225 comparable transcriptional regulation in both genotypes 4 and 24 hrs after damage infliction  
226 (**Supplementary Fig. 4d**). Having established that CEP-1 activation occurs independently of  
227 *ufd-2*, we wondered if UFD-2 foci formation might be dependent on CEP-1. Strikingly, loss  
228 of CEP-1 prevented UFD-2 foci induction after IR (**Fig. 5d**), whereas UFD-2 protein  
229 expression remained unaffected (**Supplementary Fig. 5b**). Consistently, a double mutant of  
230 the two pro-apoptotic CEP-1 effectors, *egl-1; ced-13*, which is similarly defective in DNA  
231 damage-induced apoptosis as *cep-1* mutants<sup>40</sup>, phenocopied the *cep-1* defect in UFD-2 foci  
232 formation after DNA damage (**Fig. 5d and Supplementary Fig. 5a**). To further confirm a  
233 direct role of CEP-1 in UFD-2 foci formation, we enhanced CEP-1 activity by employing a  
234 *gld-1(op236)* mutation, previously shown to increase CEP-1 levels<sup>13</sup>. *gld-1* mutants indeed  
235 displayed strongly elevated UFD-2 foci, supporting the idea that CEP-1 promotes UFD-2

236 focal accumulation. The *cep-1; gld-1* double mutant displayed a similar number of UFD-2  
237 foci as wild-type germ cells (**Fig. 5d and Supplementary Fig. 5a**). One potential explanation  
238 for the failure of *cep-1* to completely suppress the foci formation in *gld-1* might be the  
239 numerous additional target mRNAs of GLD-1<sup>41,42</sup>. Of note, the failure of *cep-1* to initiate  
240 apoptosis does not affect repair activity as IR-induced embryonic lethality has previously  
241 been shown to remain unaffected<sup>13</sup>. Consistently, we found that RAD-51 foci disassembly 16  
242 hrs after damage induction was as efficient in *cep-1* and *gld-1* mutants as in wild-type  
243 (**Supplementary Fig. 5c**). In contrast to the loss of CEP-1 signaling, UFD-2 foci formation  
244 was unaltered in apoptosis deficient *ced-3* and *ced-4* mutant worms (**Fig. 5d**), emphasizing  
245 the necessity of CEP-1 activity for UFD-2 foci formation rather than the apoptotic process in  
246 general. Taken together, UFD-2 seems to act downstream of the pro-apoptotic signaling  
247 cascade.

248

#### 249 **Resolution of RAD-51 is linked to apoptotic signaling**

250 We next wished to investigate the role of UFD-2 in the removal of RAD-51 foci and its  
251 consequence on apoptosis. Germline-specific expression of UFD-2::GFP in transgenic *ufd-2*  
252 deletion mutants rescued the delay of RAD-51 removal from DNA (**Fig. 6a**). Increased RAD-  
253 51 retention occurred in moderately RAD-51::GFP overexpressing worms after 24 hrs of IR  
254 compared to wild-type (**Fig. 6a**). Importantly, the retention of RAD-51 filaments either by  
255 loss of *ufd-2* or by RAD-51 overexpression strictly correlated with reduced apoptosis levels  
256 (**Fig. 6b**). Despite the elevated RAD-51 protein levels, the GFP transgenic line possessed  
257 normal repair capacity as assessed by embryonic survival after IR thus suggesting that the  
258 reduced apoptosis is not related to enhanced removal of DSBs (**Supplementary Fig. 6a**).  
259 Conversely, the *atx-3* mutant, which displayed increased UFD-2 foci and apoptosis after DNA  
260 damage, showed decreased RAD-51 retention 16 hrs after IR (**Supplementary Fig. 6b**). To

261 test whether elevated RAD-51 levels might directly account for the reduced apoptosis  
262 observed in *ufd-2* mutants or upon overexpression of RAD-51, we depleted RAD-51 by RNAi  
263 knockdown. Indeed, *rad-51*(RNAi) in *ufd-2* mutant or RAD-51::GFP expressing worms  
264 reverted the apoptosis defect following IR treatment (**Fig. 6c**). Importantly, *rad-51*(RNAi)  
265 also reduced embryonic survival after IR in wild-type and *rad-51* mutant worms  
266 (**Supplementary Fig. 6c**). We further validated the role of RAD-51 filaments in suppressing  
267 the apoptotic response by inhibition of RAD-51 filament formation with the RAD-51 inhibitor  
268 B02<sup>43</sup>. Similarly to reduced RAD-51 levels, treatment with B02 reverted the apoptosis  
269 phenotype of *ufd-2* deletion mutants or the RAD-51 overexpression line (**Fig. 6d**), suggesting  
270 that RAD-51 accumulation directly antagonizes apoptotic signaling. Moreover, *rad-51*  
271 heterozygous mutants with reduced RAD-51 levels reverted the apoptosis defect of *ufd-2*  
272 mutants (**Fig. 6e**). In summary, these observations support the idea that UFD-2 contributes to  
273 resolution of DNA repair sites and that retention of RAD-51 filaments leads to inhibition of  
274 apoptosis (**Fig. 6f**).

275

## 276 **DISCUSSION**

277 In this study we uncovered a ubiquitin dependent process that facilitates the communication  
278 between DNA repair and the apoptotic response. We implicated the E4 ubiquitin ligase UFD-  
279 2 as a central regulator for the spatiotemporal coordination of both processes. Our data  
280 suggest that defects in timely proceeding of HR either by failure to resolve HJs as previously  
281 demonstrated<sup>8,9</sup> or by aberrant retention of RAD-51 foci at the chromatin caused by loss of  
282 UFD-2 as shown here, halt the apoptotic response. Conversely, RAD-51 filament assembly  
283 and pro-apoptotic signaling by the p53 tumor suppressor homolog CEP-1 are both required  
284 for the formation of UFD-2-specific hubs that we define by the presence of proteolytic factors  
285 of the UPS machinery (**Fig. 6f**). We propose that these degradation hubs calibrate the  
286 proceeding of the DNA repair machinery with apoptotic activity via modulation of ubiquitin

287 signaling. Such a calibration might allow gaining time for ongoing HR repair when CEP-1  
288 dependent apoptotic signaling has already been triggered. Indeed, CEP-1 activity can be  
289 detected within the first hour following IR treatment<sup>40</sup>, while the rapidly formed RAD-51 foci  
290 are turned over in the course of 24 hrs. To prevent the precocious demise of cells that are  
291 engaged in the process of repairing DSBs, the simultaneous presence of pro-apoptotic  
292 signaling and ongoing HR requires coordination, which we propose is orchestrated at the HR  
293 repair sites through the UFD-2-ubiquitin hubs that might thus provide feedback to the  
294 apoptotic signaling on the status of the damage removal. The fine-tuning of ubiquitin chain  
295 topology by concerted action of UFD-2, the E3 ligase HECD-1 and the hydrolase ATX-3 at  
296 HR sites might indeed constitute a versatile signaling tool to enable communication between  
297 the apoptotic response and DNA damage (**Fig. 6f**). Since the E3 ligase HECD-1 is required  
298 for UFD-2 hub formation and apoptosis execution, we propose that E4 activity<sup>17,31,44</sup> is  
299 providing an additional layer of regulation by editing ubiquitin chain topology. The human E4  
300 homolog UBE4B cooperates similarly with the HECT domain E3 ligase TRIP12 in substrate  
301 ubiquitylation, suggesting the existence of a conserved signaling pathway<sup>30</sup>. In support of this  
302 idea, TRIP12 fine-tunes ubiquitin controlled events at DSBs<sup>45</sup> and recent reports linked  
303 UBE4B to different cancer types, highlighting the relevance of ubiquitin signaling in the  
304 decision between DNA damage and apoptosis response<sup>46-49</sup>. Disassembly of RAD-51  
305 filaments might involve the ubiquitin-selective segregase CDC-48/p97, which was recently  
306 implicated in chromatin associated protein degradation<sup>26,27</sup>. Moreover, Cdc48 was shown to  
307 limit RAD51 occupancy on DNA<sup>50</sup>. In agreement with this notion, CDC-48 binding is  
308 required for UFD-2 to trigger DNA damage induced cell death (**Fig. 3g**). Defects in DNA  
309 repair and apoptosis are especially relevant in tumor formation. Thus, understanding the  
310 conserved role of UFD-2/UBE4B in response to IR induced DNA damage might open new  
311 therapeutic directions for drug development and cancer treatment.

312 **Acknowledgements** We thank Y. Kohara, M. Marr, the *Caenorhabditis* Genetics Center  
313 (funded by the NIH National Center for Research Resources), the Bloomington Stock Center,  
314 the Dana-Farber Cancer Institute, Addgene and Geneservice Ltd for antibodies, plasmids,  
315 cDNAs, and strains; K. Gödderz, A. Lisowski, and E. Stellbrink for technical help. We thank  
316 A. Franz and A. Gutschmidt for critical reading of the manuscript. We thank K. Ramadan and  
317 Y. Shiloh for insightful discussions on the project and exchange of unpublished results. This  
318 work was supported by a Wellcome Trust Senior Research award (090944/Z/09/Z) to A.G.,  
319 grants of the German-Israeli Foundation (GIF 1104-68.11/2010), the Deutsche  
320 Forschungsgemeinschaft (EXC 229, SFB 829, SFB 670, and KFO 286), the European  
321 Research Council (ERC Starting grant 260383), Marie Curie (FP7 ITN CodeAge 316354,  
322 aDDRes 316390, MARRIAGE 316964), and the Bundesministerium für Forschung und  
323 Bildung (Sybacol FKZ0315893A-B) to B.S., and the Deutsche Forschungsgemeinschaft  
324 (EXC 229, HO 2541/8-1, and KFO 286) and the European Research Council (consolidator  
325 grant 616499) to T.H. In addition, this work was supported by COST Action  
326 (PROTEOSTASIS BM1307), supported by COST (European Cooperation in Science and  
327 Technology).

328

329 **Author Contributions** L.A. and M.S. designed, performed and analyzed the experiments.  
330 W.P. performed *in vitro* ubiquitylation assays. É.K. generated ATX-3 antibody. A.G. and B.S.  
331 designed and performed the RNAi screen. B.S. and T.H. supervised the design and data  
332 interpretation. L.A., B.S., and T.H. wrote the manuscript. All authors discussed the results and  
333 commented on the manuscript.

334

335 **Author Information** Reprints and permissions information is available at  
336 [www.nature.com/reprints](http://www.nature.com/reprints). The authors declare no competing financial interests.  
337 Correspondence and requests for materials should be addressed to B.S.  
338 ([bjoern.schumacher@uni-koeln.de](mailto:bjoern.schumacher@uni-koeln.de)) or T.H. ([thorsten.hoppe@uni-koeln.de](mailto:thorsten.hoppe@uni-koeln.de)).

339

## 340 REFERENCES

- 341 1. Hoeijmakers, J.H. Genome maintenance mechanisms for preventing cancer. *Nature*  
342 **411**, 366-374 (2001).
- 343 2. Clejan, I., Boerckel, J. & Ahmed, S. Developmental modulation of nonhomologous  
344 end joining in *Caenorhabditis elegans*. *Genetics* **173**, 1301-1317 (2006).
- 345 3. Lemmens, B.B. & Tijsterman, M. DNA double-strand break repair in *Caenorhabditis*  
346 *elegans*. *Chromosoma* **120**, 1-21 (2011).
- 347 4. Bizard, A.H. & Hickson, I.D. The dissolution of double Holliday junctions. *Cold*  
348 *Spring Harb Perspect Biol* **6**, a016477 (2014).
- 349 5. Matos, J. & West, S.C. Holliday junction resolution: regulation in space and time.  
350 *DNA Repair (Amst)* **19**, 176-81 (2014).
- 351 6. Schwartz, E.K. & Heyer, W.D. Processing of joint molecule intermediates by  
352 structure-selective endonucleases during homologous recombination in eukaryotes.  
353 *Chromosoma* **120**, 109-27 (2011).
- 354 7. West, S.C. et al. Resolution of Recombination Intermediates: Mechanisms and  
355 Regulation. *Cold Spring Harb Symp Quant Biol* (2015).
- 356 8. Bailly, A.P. et al. The *Caenorhabditis elegans* homolog of Gen1/Yen1 resolvases links  
357 DNA damage signaling to DNA double-strand break repair. *PLoS genetics* **6**(2010).
- 358 9. Silva, N., Adamo, A., Santonicola, P., Martinez-Perez, E. & Volpe, L.A. Pro-  
359 crossover factors regulate damage-dependent apoptosis in the *Caenorhabditis elegans*  
360 germ line. *Cell Death & Differentiation* **20**, 1209-1218 (2013).
- 361 10. Gartner, A., Milstein, S., Ahmed, S., Hodgkin, J. & Hengartner, M.O. A conserved  
362 checkpoint pathway mediates DNA damage--induced apoptosis and cell cycle arrest in  
363 *C. elegans*. *Molecular cell* **5**, 435-443 (2000).

- 364 11. Schumacher, B., Hofmann, K., Boulton, S. & Gartner, A. The C. elegans homolog of  
365 the p53 tumor suppressor is required for DNA damage-induced apoptosis. *Current*  
366 *biology : CB* **11**, 1722-1727 (2001).
- 367 12. Derry, W.B., Putzke, A.P. & Rothman, J.H. Caenorhabditis elegans p53: role in  
368 apoptosis, meiosis, and stress resistance. *Science* **294**, 591-5 (2001).
- 369 13. Schumacher, B. et al. Translational repression of C. elegans p53 by GLD-1 regulates  
370 DNA damage-induced apoptosis. *Cell* **120**, 357-368 (2005).
- 371 14. Reinke, V. et al. A global profile of germline gene expression in C. elegans. *Molecular*  
372 *cell* **6**, 605-616 (2000).
- 373 15. Vermezovic, J., Stergiou, L., Hengartner, M.O. & d'Adda di Fagagna, F. Differential  
374 regulation of DNA damage response activation between somatic and germline cells in  
375 Caenorhabditis elegans. *Cell death and differentiation* **19**, 1847-1855 (2012).
- 376 16. Johnson, E.S., Ma, P.C.M., Ota, I.M. & Varshavsky, A. A Proteolytic Pathway That  
377 Recognizes Ubiquitin as a Degradation Signal. *Journal of Biological Chemistry* **270**,  
378 17442-17456 (1995).
- 379 17. Koegl, M. et al. A novel ubiquitination factor, E4, is involved in multiubiquitin chain  
380 assembly. *Cell* **96**, 635-644 (1999).
- 381 18. Saeki, Y., Tayama, Y., Toh-e, A. & Yokosawa, H. Definitive evidence for Ufd2-  
382 catalyzed elongation of the ubiquitin chain through Lys48 linkage. *Biochemical and*  
383 *biophysical research communications* **320**, 840-845 (2004).
- 384 19. Hoppe, T. Multiubiquitylation by E4 enzymes: 'one size' doesn't fit all. *Trends*  
385 *Biochem Sci* **30**, 183-7 (2005).
- 386 20. Kuhlbrodt, K. et al. The Machado-Joseph disease deubiquitylase ATX-3 couples  
387 longevity and proteostasis. *Nat Cell Biol* **13**, 273-81 (2011).
- 388 21. Okumura, F., Hatakeyama, S., Matsumoto, M., Kamura, T. & Nakayama, K.I.  
389 Functional regulation of FEZ1 by the U-box-type ubiquitin ligase E4B contributes to  
390 neuritogenesis. *The Journal of biological chemistry* **279**, 53533-53543 (2004).
- 391 22. Hodgkin, J., Horvitz, H.R. & Brenner, S. Nondisjunction Mutants of the Nematode  
392 CAENORHABDITIS ELEGANS. *Genetics* **91**, 67-94 (1979).
- 393 23. Janiesch, P.C. et al. The ubiquitin-selective chaperone CDC-48/p97 links myosin  
394 assembly to human myopathy. *Nat Cell Biol* **9**, 379-90 (2007).
- 395 24. Rape, M. et al. Mobilization of processed, membrane-tethered SPT23 transcription  
396 factor by CDC48(UFD1/NPL4), a ubiquitin-selective chaperone. *Cell* **107**, 667-77  
397 (2001).

- 398 25. Richly, H. et al. A series of ubiquitin binding factors connects CDC48/p97 to substrate  
399 multiubiquitylation and proteasomal targeting. *Cell* **120**, 73-84 (2005).
- 400 26. Meerang, M. et al. The ubiquitin-selective segregase VCP/p97 orchestrates the  
401 response to DNA double-strand breaks. *Nat Cell Biol* **13**, 1376-82 (2011).
- 402 27. Acs, K. et al. The AAA-ATPase VCP/p97 promotes 53BP1 recruitment by removing  
403 L3MBTL1 from DNA double-strand breaks. *Nat Struct Mol Biol* **18**, 1345-50 (2011).
- 404 28. Dantuma, N.P. & Hoppe, T. Growing sphere of influence: Cdc48/p97 orchestrates  
405 ubiquitin-dependent extraction from chromatin. *Trends Cell Biol* **22**, 483-91 (2012).
- 406 29. Baek, G.H., Kim, I. & Rao, H. The Cdc48 ATPase modulates the interaction between  
407 two proteolytic factors Ufd2 and Rad23. *Proc Natl Acad Sci U S A* **108**, 13558-63  
408 (2011).
- 409 30. Park, Y., Yoon, S.K. & Yoon, J.-B.B. TRIP12 functions as an E3 ubiquitin ligase of  
410 APP-BP1. *Biochemical and biophysical research communications* **374**, 294-298  
411 (2008).
- 412 31. Liu, G., Rogers, J., Murphy, C.T. & Rongo, C. EGF signalling activates the ubiquitin  
413 proteasome system to modulate *C. elegans* lifespan. *The EMBO journal* **30**, 2990-3003  
414 (2011).
- 415 32. Shaye, D.D. & Greenwald, I. OrthoList: a compendium of *C. elegans* genes with  
416 human orthologs. *PloS one* **6**(2011).
- 417 33. Marechal, A. & Zou, L. RPA-coated single-stranded DNA as a platform for post-  
418 translational modifications in the DNA damage response. *Cell Res* **25**, 9-23 (2015).
- 419 34. Boulton, S.J. et al. BRCA1/BARD1 orthologs required for DNA repair in  
420 *Caenorhabditis elegans*. *Curr Biol* **14**, 33-9 (2004).
- 421 35. Solinger, J.A., Kiiianitsa, K. & Heyer, W.D. Rad54, a Swi2/Snf2-like recombinational  
422 repair protein, disassembles Rad51:dsDNA filaments. *Mol Cell* **10**, 1175-88 (2002).
- 423 36. Agostinho, A. et al. Combinatorial regulation of meiotic holliday junction resolution  
424 in *C. elegans* by HIM-6 (BLM) helicase, SLX-4, and the SLX-1, MUS-81 and XPF-1  
425 nucleases. *PLoS genetics* **9**(2013).
- 426 37. O'Neil, N.J. et al. Joint molecule resolution requires the redundant activities of MUS-  
427 81 and XPF-1 during *Caenorhabditis elegans* meiosis. *PLoS Genet* **9**, e1003582  
428 (2013).
- 429 38. Hofmann, E.R. et al. *Caenorhabditis elegans* HUS-1 is a DNA damage checkpoint  
430 protein required for genome stability and EGL-1-mediated apoptosis. *Current biology*  
431 : *CB* **12**, 1908-1918 (2002).



- 432 39. Horvitz, H.R. Genetic control of programmed cell death in the nematode  
433 *Caenorhabditis elegans*. *Cancer Res* **59**, 1701s-1706s (1999).
- 434 40. Schumacher, B. et al. *C. elegans* ced-13 can promote apoptosis and is induced in  
435 response to DNA damage. *Cell Death Differ* **12**, 153-61 (2005).
- 436 41. Lee, M.H. & Schedl, T. Identification of in vivo mRNA targets of GLD-1, a maxi-KH  
437 motif containing protein required for *C. elegans* germ cell development. *Genes &*  
438 *development* **15**, 2408-2420 (2001).
- 439 42. Doh, J.H., Jung, Y., Reinke, V. & Lee, M.-H.H. *C. elegans* RNA-binding protein  
440 GLD-1 recognizes its multiple targets using sequence, context, and structural  
441 information to repress translation. *Worm* **2**(2013).
- 442 43. Huang, F. & Mazin, A.V. A small molecule inhibitor of human RAD51 potentiates  
443 breast cancer cell killing by therapeutic agents in mouse xenografts. *PloS one* **9**(2014).
- 444 44. Park, Y., Yoon, S.K. & Yoon, J.-B.B. The HECT domain of TRIP12 ubiquitinates  
445 substrates of the ubiquitin fusion degradation pathway. *The Journal of biological*  
446 *chemistry* **284**, 1540-1549 (2009).
- 447 45. Gudjonsson, T. et al. TRIP12 and UBR5 suppress spreading of chromatin  
448 ubiquitylation at damaged chromosomes. *Cell* **150**, 697-709 (2012).
- 449 46. Krona, C. et al. Screening for gene mutations in a 500 kb neuroblastoma tumor  
450 suppressor candidate region in chromosome 1p; mutation and stage-specific  
451 expression in UBE4B/UFD2. *Oncogene* **22**, 2343-51 (2003).
- 452 47. Carén, H., Holmstrand, A., Sjöberg, R.M.M. & Martinsson, T. The two human  
453 homologues of yeast UFD2 ubiquitination factor, UBE4A and UBE4B, are located in  
454 common neuroblastoma deletion regions and are subject to mutations in tumours.  
455 *European journal of cancer (Oxford, England : 1990)* **42**, 381-387 (2006).
- 456 48. Zage, P.E. et al. UBE4B levels are correlated with clinical outcomes in neuroblastoma  
457 patients and with altered neuroblastoma cell proliferation and sensitivity to epidermal  
458 growth factor receptor inhibitors. *Cancer* **119**, 915-923 (2013).
- 459 49. Kloppsteck, P., Ewens, C.A., Forster, A., Zhang, X. & Freemont, P.S. Regulation of  
460 p97 in the ubiquitin-proteasome system by the UBX protein-family. *Biochim Biophys*  
461 *Acta* **1823**, 125-9 (2012).
- 462 50. Bergink, S. et al. Role of Cdc48/p97 as a SUMO-targeted segregase curbing Rad51-  
463 Rad52 interaction. *Nat Cell Biol* **15**, 526-32 (2013).
- 464
- 465

466 **FIGURE LEGENDS**

467 **Figure 1** Ubiquitin ligase activity of UFD-2 is required for apoptosis execution. **(a)**  
468 Schematic illustration of RNAi screen for identification of DNA damage-induced apoptosis  
469 mediators. After RNAi treatment worms were subjected to IR and scored for apoptotic  
470 corpses (indicated by filled arrowheads) 24 hrs later by differential interference contrast  
471 (DIC) microscopy. Representative images of 3 independent experiments. **(b)** Apoptotic  
472 corpses in worms treated with indicated RNAi constructs and exposed to different IR doses,  
473 24 hrs after treatment. Data represent mean  $\pm$  s.e.m. of 3 independent experiments. *n* varied  
474 from 2-11 animals, see **Supplementary Table 1**. **(c)** Representative images of late pachytene  
475 cells of *C. elegans* germline 24 hrs after IR treatment (0, 60 Gy). Filled arrowheads indicate  
476 apoptotic corpses. Scale bar 5  $\mu$ m. Representative images of 3 independent experiments. **(d)**  
477 Analysis of DNA damage induced apoptosis 24 hrs after IR treatment (0, 30 or 60 Gy) of  
478 indicated genotypes. Center lines show the medians; box limits indicate the 25th and 75th  
479 percentiles as determined by R software; whiskers extend 1.5 times the interquartile range  
480 from the 25th and 75th percentiles, outliers are represented by dots. The notches are defined  
481 as  $\pm 1.58 \cdot \text{IQR} / \sqrt{n}$  and represent the 95% confidence interval for each median. Non-  
482 overlapping notches give roughly 95% confidence that two medians differ. Data of 5  
483 independent experiments. *n* varied from 69-80 animals, see **Supplementary Table 1**. **(e)**  
484 Auto-ubiquitylation of UFD-2 with UFD-2 (wild-type) or UFD-2<sup>P951A</sup> as ubiquitin ligases.  
485 Representative immunoblot of 3 independent experiments. **(f)** Analysis of DNA damage  
486 induced apoptosis 24 hrs after IR treatment (0, 60 Gy) of indicated genotypes. Statistics as in  
487 **Fig. 1d**. Data of 3 independent experiments. *n* varied from 36-63 animals, see  
488 **Supplementary Table 1**.

489 **Figure 2** UFD-2 forms foci late after IR treatment. **(a)** Representative images of worm  
490 germlines of indicated genotypes stained with  $\alpha$ -UFD-2 antibody and DAPI 24 hrs after IR

491 treatment (60 Gy). Filled arrowhead indicate nuclei with UFD-2 foci. Scale bar, 5  $\mu$ m.  
492 Representative images of 3 independent experiments and (b) corresponding quantification of  
493 UFD-2 foci in pachytene region of germlines. Data show means  $\pm$  s.e.m. of 12 independent  
494 experiments.  $n = 231$  animals (wt 0 Gy) and  $n = 280$  animals (wt 60 Gy). (c) Representative  
495 images of worm germlines of indicated genotypes stained with GFP-booster and DAPI 24 hrs  
496 after IR treatment (60 Gy). Filled arrowheads indicate nuclei with UFD-2 foci. Scale bar, 5  
497  $\mu$ m. Representative images of 3 independent experiments and (d) corresponding  
498 quantification of UFD-2 foci in pachytene region of germlines. Data show means  $\pm$  s.e.m. of 3  
499 independent experiments.  $n$  varied from 34-51 animals, see **Supplementary Table 1**.

500 **Figure 3** UPS factors accumulate in UFD-2 hubs and balance apoptotic signaling.  
501 Representative images of (a) *ufd-2(tm1380); UFD-2::GFP* and (b) *ufd-2(tm1380); UFD-*  
502 *2<sup>P951A</sup>::GFP* immunostained with indicated antibodies 24 hrs after IR (Gy 60). The boxed area  
503 is three times magnified (3x zoom).  $\alpha$ -alpha SU,  $\alpha$ -Proteasome 20S alpha subunits. Scale bars,  
504 5  $\mu$ m. Representative images of 3 independent experiments. (c) Representative images of  
505 worm germlines of indicated genotypes immunostained with  $\alpha$ -UFD-2 antibody and DAPI 24  
506 hrs after IR treatment (60 Gy). Filled and empty arrowhead indicated nuclei positive or  
507 negative for UFD-2 foci, respectively. Scale bar, 5  $\mu$ m Representative images of 3  
508 independent experiments and (d) corresponding quantification of UFD-2 foci in pachytene  
509 region of germlines. Data show means  $\pm$  s.e.m. of 3 independent experiments.  $n$  varied from  
510 36-107 animals, see **Supplementary Table 1**. (e,f,g) Analysis of DNA damage induced  
511 apoptosis 24 hrs after IR treatment (0, 60 Gy) of indicated genotypes. Statistics as in **Fig. 1d**.  
512 Data of 3 independent experiments.  $n$  varied from 39-52 animals for (e), 38-51 animals for (f)  
513 and 34-74 animals for (g), see **Supplementary Table 1**.

514 **Figure 4** Loss of *ufd-2* delays DSB repair processing. (a) Schematic illustration of DNA DSB  
515 repair by HR in *C. elegans*. Upon DSB induction RPA binds resected single stranded DNA,

516 BRD-1 acts together with BRCA-1 at DSB site, RPA is exchanged for RAD-51, which  
517 mediates strand invasion, Gen-1 resolves HJ resulting in repaired DSB. Names in brackets  
518 indicate human homologues. **(b)** Representative images of *BRD-1::GFP* and *RPA-1::GFP*  
519 germlines stained with  $\alpha$ -UFD-2 and DAPI 24 hrs after IR treatment (60 Gy). Scale bar, 5  $\mu$ m.  
520 Representative images of 3 independent experiments. **(c)** Representative images of wild-type  
521 and *ufd-2(tm1380)* germlines isolated 16 hrs after IR treatment (20 Gy), stained with  $\alpha$ -RAD-  
522 51 and DAPI. Filled arrowheads indicate nuclei positive for RAD-51 staining. Scale bar, 10  
523  $\mu$ m. Representative images of 3 independent experiments. **(d)** Quantification of germ cells  
524 positive for RAD-51 staining of wild-type and *ufd-2(tm1380)* worms treated with IR (0 Gy)  
525 and isolated after 1hr or treated with IR (20 Gy) and isolated after 1, 7, 16, 48 hrs. Data show  
526 means  $\pm$  s.e.m. of 3 independent experiments. *n* varied from 35-43 animals, see  
527 **Supplementary Table 1**. The triple asterisk indicates *P* value of  $\leq 0.001$  in two-tailed  
528 Student's *t*-test.

529 **Figure 5** UFD-2 foci in repair and apoptosis after DNA damage. **(a)** Schematic illustration of  
530 apoptosis pathway in *C. elegans*. Names in brackets indicate human homologues. **(b,c,d)**  
531 Quantification of UFD-2 foci in pachytene region of germlines of indicated genotypes  
532 isolated 24 hrs after irradiation (60 Gy). Data show means  $\pm$  s.e.m. of 3 independent  
533 experiments. *n* varied from 30-113 animals for **(b)**, 34-92 animals for **(c)** and 20-202 animals  
534 for **(d)**, see **Supplementary Table 1**.

535 **Figure 6** UFD-2 coordinates communication between repair and apoptosis after DNA  
536 damage. **(a)** Quantification of germ cells positive for RAD-51 staining of indicated genotypes  
537 treated with IR (0 or 20 Gy) and isolated after 24 hrs. Data show means  $\pm$  s.e.m. of 3  
538 independent experiments. *n* varied from 34-63 animals, see **Supplementary Table 1**. The  
539 triple asterisk indicates *P* value of  $\leq 0.001$  in two-tailed Student's *t*-test. **(b)** Analysis of DNA  
540 damage induced apoptosis 24 hrs after IR treatment (0, 60 Gy) of indicated genotypes.

541 Statistics as in **Fig. 1d**. Data of 3 independent experiments. *n-values* varied from 61-82  
542 animals, see **Supplementary Table 1**. (c,d,e) Analysis of DNA damage induced apoptosis 24  
543 hrs after IR treatment (0, 60 Gy) of (c) *ufd-2* and RAD-51::GFP treated with *rad-51* or control  
544 RNAi or (d) wild-type, *ufd-2*, and RAD-51::GFP worms treated with RAD51 inhibitor B02  
545 (200 mM) or (e) indicated genotypes. Statistics as in **Fig. 1d**. Data of 3 independent  
546 experiments. *n-values* varied from 30-47 animals for (c), 28-69 animals for (d) and 29-40  
547 animals for (e), see **Supplementary Table 1**. (f) Model for the coordination between HR and  
548 apoptotic signaling by UFD-2. DSB repair triggers RAD-51 accumulation at ssDNA to  
549 facilitate homology pairing. After efficient strand invasion RAD-51 is removed and HJ are  
550 resolved by HJ processing enzymes (GEN-1, MUS-81 and XPF-1). UFD-2 supports RAD-51  
551 dissociation from DSB at advanced time points. Ongoing repair is reflected by the presence of  
552 UFD-2 containing hubs late after IR. These ubiquitylation hubs contain processivity factors  
553 like CDC-48 and proteasome (not shown). Interaction between UFD-2 and CDC-48 is  
554 necessary to transduce a pro-apoptotic signal. UFD-2 hub formation is fine-tuned by the E3  
555 ligase HECD-1, the DUB ATX-3, and pro-apoptotic CEP-1/p53 signaling.

556 **METHODS**

557 ***C. elegans* strains.** *C. elegans* strains were cultured at 20 °C on nematode growth medium  
558 (NGM) and fed with *Escherichia coli* (*E. coli*) strain OP50 according to standard procedures  
559 <sup>51</sup>. The Bristol strain N2 was used as wild-type. Mutants and transgenic animals used in this  
560 study are listed in the following: *mus-81(tm1937) I*, *rad-54&snx-3(ok615) I/hT2 [bli-4(e937)*  
561 *let-?(q782) qIs48] (I;III)*, *cep-1(lg12501)I*, *ced-1(e1735)I*, *gld-1(op236)I*, *ufd-2(tm1380)II*,  
562 *ufd-2(hh1)II*, *xpf-1(tm2842) II*, *gen-1(tm2940)III*, *ced-4(n1162) III*, *hecd-1(tm2371)IV*, *rad-*  
563 *51(ok2218) IV/nT1[qIs51](IV;V)*, *ced-3(n717) IV*, *atx-3(gk193)V*, *egl-1(n1084n3082)V*; *ced-*  
564 *13(tm536)X*, , *Is[rad-51::GFP:3xFLAG]*, *gla-3(op216)I*, *hus-1(op241)I*, *unc-119(ed3)III*;  
565 *gtIs[unc-119(+)*, *Ppie-1::GFP::rpa-1::pie-1-3'UTR]*, *hhIs121[unc-119(+)*, *Pmex-5::ufd-*  
566 *2::GFP::tbb-2 3'UTR]*, *hhIs135[unc-119(+)*, *Pmex-5 (w/o ATG)::ufd-2 (w/o TAA,*  
567 *P951A)::(Gly)5Ala::gfp F64LS65T(w introns/stop)::tbb-2 3'UTR]*, *hhIs134[unc-119(+)*,  
568 *Pmex-5::ufd-2 (C448Y)::GFP::tbb-2 3'UTR]*.

569 The transgenic lines *hhIs121*, *hhIs134*, and *hhIs135* were generated for this study. Briefly,  
570 fosmid WRM0621dE05 was used as template to obtain the genomic sequence of *ufd-2* that  
571 was cloned together with ppJA252, pJA257 into pCG150 containing the *unc-119(+)* marker  
572 for selection of transgenic worms <sup>52</sup>. *ufd-2* was modified by directed mutagenesis to create  
573 *ufd-2<sup>P951A</sup>* or *ufd-2<sup>C448Y</sup>*. The constructs were bombarded into *unc-119(ed4)III* mutants as  
574 described previously <sup>53</sup>.

575 No statistical method was used to predetermine sample size. The experiments were not  
576 randomized and were not performed with blinding to the conditions of the experiments. All *n*-  
577 values are specified in **Supplementary Table 1** (for data in Fig. 1-6) and **Supplementary**  
578 **Table 2** (for data in Supplementary Fig. 1-6).

579 **Ionizing radiation.** Synchronized hermaphrodites were grown until L4 stage and irradiated  
580 with the corresponding dose (Radiation source: 120-kV X-rays (25 mA; 0.5mm Alu-filter;  
581 ISOVOLT 160 M1/10-55, GE Sensing & Inspection Technologies) or Biobeam 8000 using  
582 Cs137 as radiation source).

583 **RNAi treatment.** RNA interference was performed using the feeding method <sup>54</sup>. Three P0  
584 worms were placed on IPTG (isopropylthiogalactoside) and ampicillin-containing NGM-  
585 plates seeded with *E. coli* [HT115(DE3)] expressing double-stranded RNA (dsRNA) and  
586 incubated at 15°C for 72 hrs. Three single F1 worms were transferred each to a new, freshly  
587 seeded plate and allowed to lay eggs for approximately 20 hrs. F1 worms were removed and  
588 F2 worms were allowed to grow up to the L4 stage, treated with ionizing radiation and  
589 analyzed for radiation induced apoptosis. Clones in RNAi feeding vectors were provided by  
590 Marc Vidal of Dana Farber Cancer Center.

591 **Apoptotic corpses.** For physiological apoptosis analysis, synchronized L1 larvae were grown  
592 until L4 stage. Apoptotic corpses were scored 24 hrs later. For this, worms were mounted on  
593 3% agar pads, paralyzed with 60 nM NaN<sub>3</sub> and analysed via DIC microscopy <sup>55</sup>. For DNA  
594 damage induced apoptosis worms were subjected to IR at L4 stage before apoptosis was  
595 evaluated 24 hrs later. Developmental apoptosis was assessed in L1 larvae. Therefore worms  
596 were grown until day one adulthood. 100 worms were transferred to a NGM-agar plate  
597 without *E. coli* and allowed to lay eggs until they were removed after 1 hr. Freshly hatched L1  
598 larvae were scored for apoptotic corpses <sup>56</sup>.

599 **UFD-2 foci.** Synchronized worms were grown until L4 larvae stage and irradiated with 0 and  
600 60 Gy. 24 hrs later, germlines were isolated and immunostained. Number of UFD-2 foci was  
601 scored in all focal planes in pachytene germ cells. One germline per worm was scored.

602 **Protein expression and purification.** cDNAs encoding *ufd-2b*, *ufd-2b*<sup>C448Y</sup>, and *ufd-2b*<sup>P951A</sup>  
603 were cloned into the pET-21d expression vector (Novagen) and pGex4T1 (GE Healthcare).  
604 Recombinant proteins were expressed in *E. coli* strain BL21 Codon Plus (Novagen) and  
605 purified using the ÄKTA purifier system (GE Healthcare).

606 **Antibody production.** His-tagged purified proteins (UFD-2, ATX-3<sup>20</sup>) were used for  
607 immunization of rabbits and anti-sera were affinity purified using respective GST-tagged  
608 recombinant proteins (BioGenes). For validation see **Supplementary Fig. 2a** and **3d**,  
609 respectively.

610 **Preparation of worm lysates.** Synchronized L1 larvae were grown on NGM-agar plates with  
611 OP50 bacteria until they reached adulthood. Worm lysates used for SDS-PAGE were either  
612 prepared from a distinct number of worms (n=150) or by washing worms from NGM-agar  
613 plates followed by multiple washing step with M9 buffer [3 g/l KH<sub>2</sub>P0<sub>4</sub>, 6 g/l Na<sub>2</sub> HPO<sub>4</sub>, 5  
614 g/l NaCl, 1 mM Mg S0<sub>4</sub> (added after sterilization)], until bacteria were removed. The samples  
615 were heated to 95°C for 5 min and subsequently shock-frozen in liquid nitrogen. After  
616 thawing, samples were subjected to sonication (two times for 15 s, on ice; 50% power;  
617 Sonopuls UW 2200, Bandelin) and taken up in 4 x SDS sample buffer followed by  
618 centrifugation at 15,000 rpm for 10 min.

619 **Immunotechniques.** Immunostaining of isolated germlines was done according to the  
620 ‘freeze-crack’ protocol. Worms were dissected onto polylysine-coated slides (Thermo  
621 Scientific) in 60 nM NaN<sub>3</sub> to isolate germlines and fixed in fixation buffer (3.7 %  
622 Formaldehyde, 0.2 % Tween 20) for 10 min with subsequent shock freezing in liquid  
623 nitrogen. This was followed by incubation in 1:1 mixture of methanol and acetone at -20 °C  
624 for 10 min. Germlines were permeabilized 3 times in 1 % PBS-Triton X-100 for 20 min  
625 followed by washing in 0.1 % PBS-Tween 20 (PBS-T) for 10 min and blocking in 10 % goat



626 serum in 0.1 % PBS-T. A specific staining protocol was followed for GFP-expressing lines  
627 avoiding freezing. Isolated germlines were fixed with fixation buffer for 10 min in PCR tubes,  
628 directly followed by permeabilization and blocking as described above. Germlines were  
629 incubated with primary antibody overnight at 4 °C (anti-UFD-2 1:3,000, anti-CDC-48  
630 1:12,000<sup>57</sup>, anti-RAD-51 1:350 (14B4, #NB100-148, Novus Biologicals<sup>58</sup>), anti-FK2-  
631 ubiquitin 1:100 (AB\_612093, #04-263, Millipore, validation on manufacturer's website), anti-  
632 Proteasome 20S alpha 1+2+3+5+6+7 antibody 1:300 (MCP231, #ab22674, abcam<sup>59</sup>), anti-  
633 ATX-3 1:700). Incubation with the fluorescently labeled secondary antibodies (#A-11037,  
634 #R37117, Life Technologies; 1:200) or GFP-booster (#GBA-488, ChromoTek; 1:400<sup>60</sup>) was  
635 done at room temperature for 1 hr. Germlines were mounted in DAPI Fluoromount-G  
636 medium (SouthernBiotech). For western blotting, worm lysates were separated by SDS-  
637 polyacrylamide gel electrophoresis (SDS-PAGE) and transferred to nitrocellulose membranes  
638 (Whatman, Protran). Membranes were blocked in 1x Roti-Block (Roth) and incubated with  
639 the primary antibodies overnight at 4 °C in Roti-Block (Roth; anti-ATX-3 1:10,000, anti-  
640 CDC-48 1:50,000<sup>57</sup>, anti-UFD-2 1:20,000, anti-CEP 1:15,000<sup>13</sup>, anti-tubulin 1:5000 (clone  
641 DM1A, Sigma-Aldrich<sup>61</sup>). Incubation with fluorescently labeled secondary antibodies (LiCor  
642 IRDye 680, #926-32222 and #926-32223, LiCor IRDye 800, #926-32212 and #926-32213,  
643 1:10,000) was done at room temperature, before detection of signals using the Li-Cor  
644 Odyssey scanner. Quantification of signal intensities was done using the Odyssey V4.0  
645 software (Li-Cor). The uncropped versions of western blots that have been used to assemble  
646 the main figures are collected in **Supplementary Fig. 7**.

647 **Immunoprecipitation *in vivo* and *in vitro*.** Worm lysates were prepared as described above  
648 and the protein concentration was determined by measuring absorption at 260nm with  
649 Nanodrop 800 UV/Vis Spectrometer. 250 µl of Dynabeads (Invitrogen) were used per  
650 reaction, washed twice with conjugation buffer [100 mM sodium phosphate, 0,15 M NaCl]

651 and resuspended in 1 ml 5 mM crosslinking reagent BS<sup>3</sup> (Thermo Scientific). Crosslinking  
652 was performed on rotation wheel for 30 min at room temperature. The reaction was stopped  
653 by adding 50 µl quenching buffer [1 M Tris/HCL, pH 7.5] followed by 15 min incubation at  
654 room temperature. The beads were washed three times with 0.5 x PBS before 50 µg α-UFD-2  
655 antibody was added and incubated for 20 min under constant rotation at room temperature.  
656 After repeated washing with 0.5 x PBS, 2.5 mg of corresponding worm protein lysate was  
657 added to the beads and incubated over night at 4 °C with rotation. For *in vitro*  
658 immunoprecipitation, antigen (UFD-2) was incubated with antibody-coupled beads for 4 hrs  
659 prior to addition of the putative binding partner (CDC-48) for an additional incubation for 4  
660 hrs. Both proteins were added in equimolar ratio (1 mM). Elution was performed as described  
661 in the manufacturer's manual.

662 **Microscopy and image acquisition.** Immunostained germlines were imaged with  
663 AxioImager.M1/Z1 microscope with Apoptome equipped with an AxioCam MRm camera  
664 (Carl Zeiss). To allow direct comparison of signal intensities, images were recorded under  
665 identical conditions. Processing of selected pictures was done in ZEN2011 and ImageJ.

666 ***In vitro* ubiquitylation assay.** UFD-2b::His, UFD-2b<sup>C448Y</sup>::GST, and UFD-2b<sup>P951A</sup>::His  
667 fusion proteins were expressed in BL21-AI *E. coli* strain and lysed in buffer A [50 mM Tris  
668 pH 7.5, 250 mM NaCl, 5 mM DTT, 1% Triton X-100, 2 mM PMSF and protease inhibitor  
669 mix; Roche]. 10 µg of the aforementioned bacterial lysate was mixed with E1 (25 ng), E2  
670 (Let-70; 400 ng), 2 µg of FLAG::ubiquitin, energy regenerating solution (Boston  
671 Biochemicals) and ubiquitin conjugation reaction Buffer (Enzo Life Sciences). Samples were  
672 incubated at 30 °C for 1.5 hrs, terminated by boiling for 5 min with SDS-sample buffer, and  
673 resolved by SDS-PAGE followed by immunoblotting using anti-UFD-2 antibodies to monitor  
674 ubiquitylation of UFD-2.

675 **Persistence of RAD-51 foci after IR.** Synchronized worms were grown until L4 larvae stage  
676 and irradiated with 0 and 20 Gy. 1 to 48 hrs later, germlines were isolated and  
677 immunostained. Z-stacks were taken of late pachytene cells of the germline. Two focal planes  
678 covering the upper and lower part of the germline were subjected to analysis by scoring each  
679 plane for RAD-51 positive cells in the last 25 nuclei of pachytene germ cells prior entering  
680 diakinesis.

681 **RNA isolation and real-time PCR.** Total RNA was isolated using TRIzol (Invitrogen) and  
682 Qiagen RNeasy kit. Briefly, worms were washed off the plates using M9 buffer [3 g/l  
683 KH<sub>2</sub>PO<sub>4</sub>, 6 g/l Na<sub>2</sub> HPO<sub>4</sub>, 5 g/l NaCl, 1 mM Mg SO<sub>4</sub> (added after sterilization)] and 600 µl  
684 TRIzol, and silica beads (1 mm diameter) were added to the samples and homogenized by  
685 Precellys tissue homogeniser. Chloroform was added and samples were vortexed vigorously  
686 before phase separation through centrifugation. The aqueous phase was transferred on the  
687 Qiagen RNeasy Mini spin column and RNA was isolated according to manufacturer's  
688 instructions. cDNA was synthesized using 200 ng total RNA and the High-Capacity cDNA  
689 Reverse Transcription Kit (Applied Biosystems). Gene expression levels were determined by  
690 real time PCR using Brilliant III Ultra-Fast SYBR Green QPCR Master Mix (Agilent  
691 Technologies) and Biorad CFX96 Real-Time PCR Detection System. Relative gene  
692 expressions were normalized to *tbg-1* (F58A4.8) mRNA levels. In the experiment three  
693 biological and three technical replicate samples were analyzed. The primer sequences used in  
694 the RT-PCR reactions are the following: *tbg-1* forward:

695 5'-GTACACTCCACTGATCTCTGCTGACAAG-3', *tbg-1* reverse:

696 5'-CTCTGTACAAGAGGCAAACAGCCATG-3'<sup>62</sup>, *egl-1* forward:

697 5'-TACTCCTCGTCTCAGGACTT-3', *egl-1* reverse: 5'-CATCGAAGTCATCGCACAT-3'.

698 **Embryonic Survival.** To determine the radiation sensitivity, L4-stage hermaphrodites were  
699 irradiated with a single dose of IR as indicated. After 12 hrs, worms were transferred to fresh

700 plates (three worms per plate, five plates in total) and allowed to lay eggs for 5 hrs. After this  
701 period, adults were removed and 24 hrs later the number of hatched and unhatched embryos  
702 was scored (number of hatched larvae normalized to results after mock-treatment). As a  
703 control for embryonic survival, a heterozygous deletion mutant lacking *rad-51* on one  
704 chromosome was used.

705 **B02 treatment.** Synchronized L1 larvae were grown as liquid culture in S Medium with heat  
706 inactivated (3 x 5 min at 65 °C, vortexing inbetween) *E. coli* strain OP50<sup>63</sup>, containing 200  
707 mM B02.

708 **Mitotic germ cell cycle arrest upon IR.** Worms were irradiated with 0 and 60 Gy at the late  
709 L4 larval stage as described previously<sup>10</sup>. 16 hours post-irradiation, worms were mounted on  
710 3% agar pads and paralyzed with 60 nM NaN<sub>3</sub> for DIC microscopy and the distal region of  
711 the germline was scored for number of nuclei in all focal planes within a defined area of 2 μm  
712 x 6 μm.

713 **Statistical analysis.** Statistical analysis was performed using Excel (Microsoft). Statistical  
714 significance was calculated with two-tailed paired Student's t-test. Box plots were generated  
715 using BoxPlotR<sup>64</sup>. Centre lines show the medians; box limits indicate the 25th and 75th  
716 percentiles as determined by R software; whiskers extend 1.5 times the interquartile range  
717 from the 25th and 75th percentiles, outliers are represented by dots. The notches are defined  
718 as  $\pm 1.58 \cdot \text{IQR} / \sqrt{n}$  and represent the 95% confidence interval for each median. Non-  
719 overlapping notches give roughly 95% confidence that two medians differ.

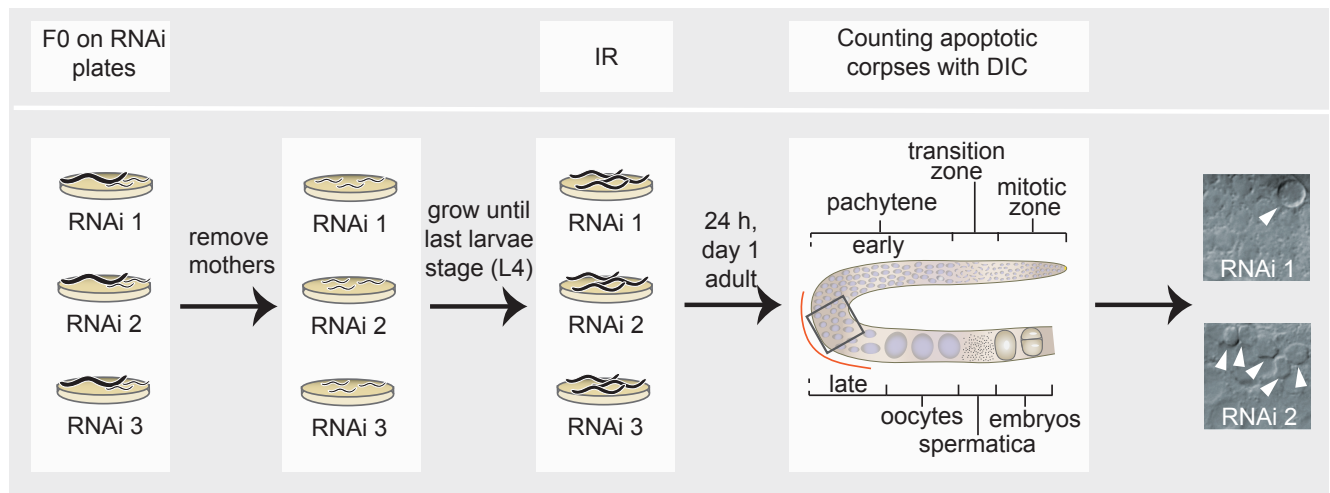
720

721 51. Brenner, S. The genetics of *Caenorhabditis elegans*. *Genetics* **77**, 71-94 (1974).

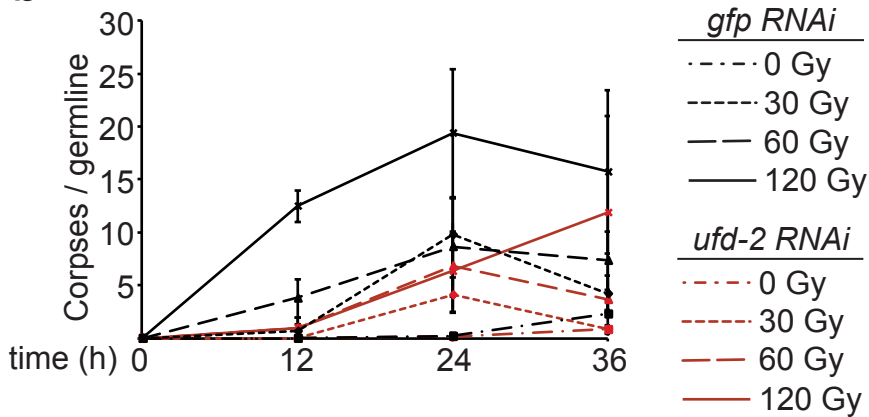
- 722 52. Zeiser, E., Frøkjær-Jensen, C., Jorgensen, E. & Ahringer, J. MosSCI and gateway  
723 compatible plasmid toolkit for constitutive and inducible expression of transgenes in  
724 the *C. elegans* germline. *PloS one* **6**(2011).
- 725 53. Praitis, V., Casey, E., Collar, D. & Austin, J. Creation of low-copy integrated  
726 transgenic lines in *Caenorhabditis elegans*. *Genetics* **157**, 1217-1226 (2001).
- 727 54. Timmons, L. & Fire, A. Specific interference by ingested dsRNA. *Nature* **395**, 854  
728 (1998).
- 729 55. Gumienny, T.L., Lambie, E., Hartweg, E., Horvitz, H.R. & Hengartner, M.O. Genetic  
730 control of programmed cell death in the *Caenorhabditis elegans* hermaphrodite  
731 germline. *Development (Cambridge, England)* **126**, 1011-1022 (1999).
- 732 56. Hengartner, M.O., Ellis, R.E. & Horvitz, H.R. *Caenorhabditis elegans* gene *ced-9*  
733 protects cells from programmed cell death. *Nature* **356**, 494-9 (1992).
- 734 57. Franz, A. et al. CDC-48/p97 coordinates CDT-1 degradation with GINS chromatin  
735 dissociation to ensure faithful DNA replication. *Mol Cell* **44**, 85-96 (2011).
- 736 58. Lans, H. et al. DNA damage leads to progressive replicative decline but extends the  
737 life span of long-lived mutant animals. *Cell Death Differ* **20**, 1709-18 (2013).
- 738 59. Stout, G.J. et al. Insulin/IGF-1-mediated longevity is marked by reduced protein  
739 metabolism. *Mol Syst Biol* **9**, 679 (2013).
- 740 60. Pourkarimi, E., Greiss, S. & Gartner, A. Evidence that CED-9/Bcl2 and CED-4/Apaf-  
741 1 localization is not consistent with the current model for *C. elegans* apoptosis  
742 induction. *Cell Death Differ* **19**, 406-15 (2012).
- 743 61. Gonczy, P. et al. Dissection of cell division processes in the one cell stage  
744 *Caenorhabditis elegans* embryo by mutational analysis. *J Cell Biol* **144**, 927-46  
745 (1999).
- 746 62. Hoogewijs, D., Houthoofd, K., Matthijssens, F., Vandesompele, J. & Vanfleteren, J.R.  
747 Selection and validation of a set of reliable reference genes for quantitative sod gene  
748 expression analysis in *C. elegans*. *BMC molecular biology* **9**, 9 (2008).
- 749 63. Lewis, J.A. & Fleming, J.T. Basic culture methods. *Methods Cell Biol* **48**, 3-29  
750 (1995).
- 751 64. Spitzer, M., Wildenhain, J., Rappsilber, J. & Tyers, M. BoxPlotR: a web tool for  
752 generation of box plots. *Nature methods* **11**, 121-122 (2014).

# Figure 1

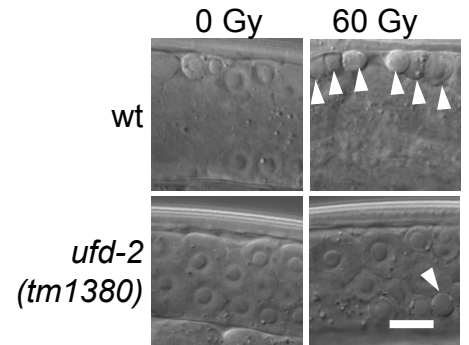
**a**



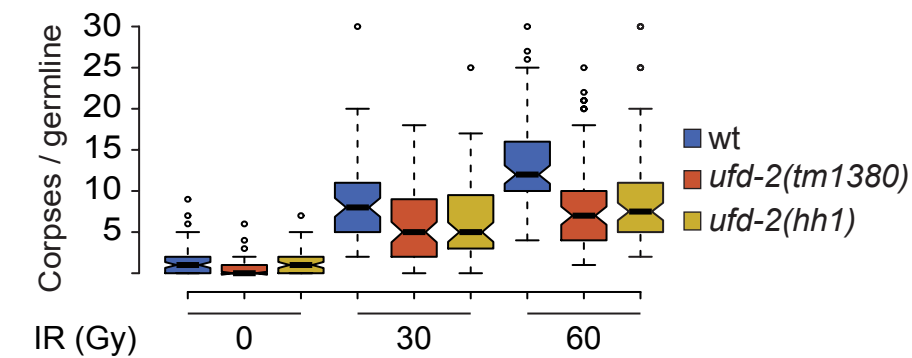
**b**



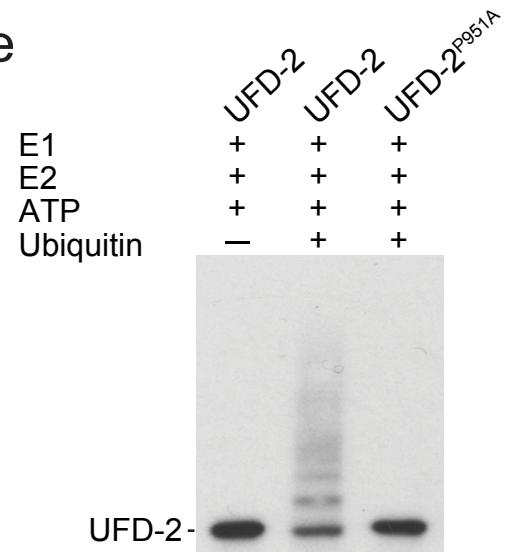
**c**



**d**



**e**



**f**

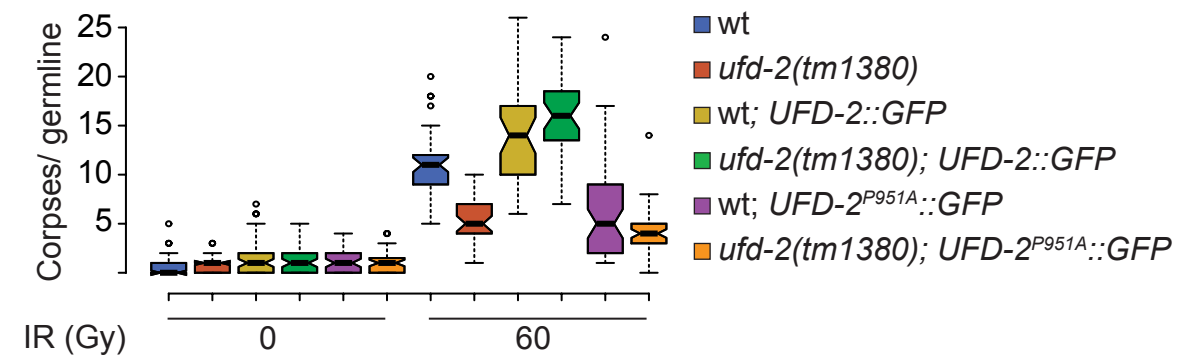
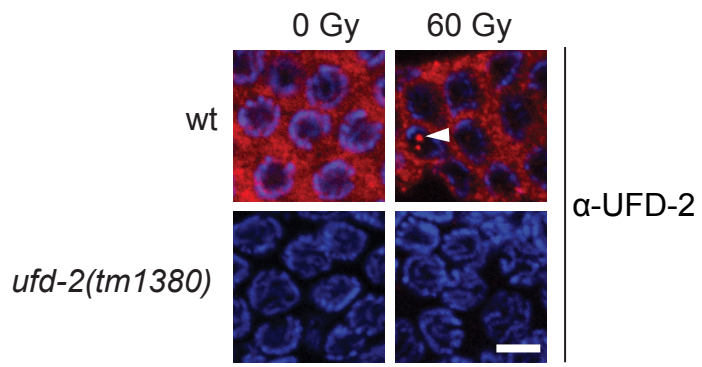
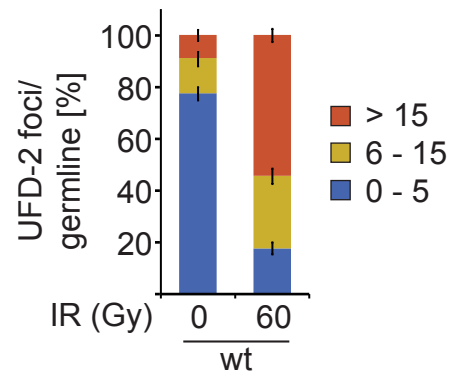


# Figure 2

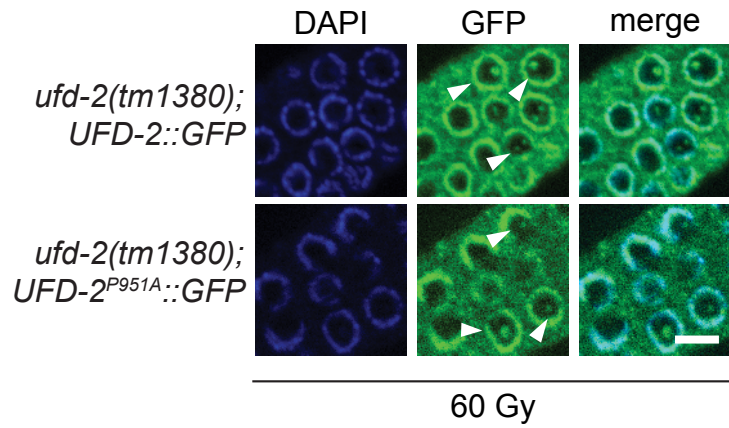
a



b



c



d

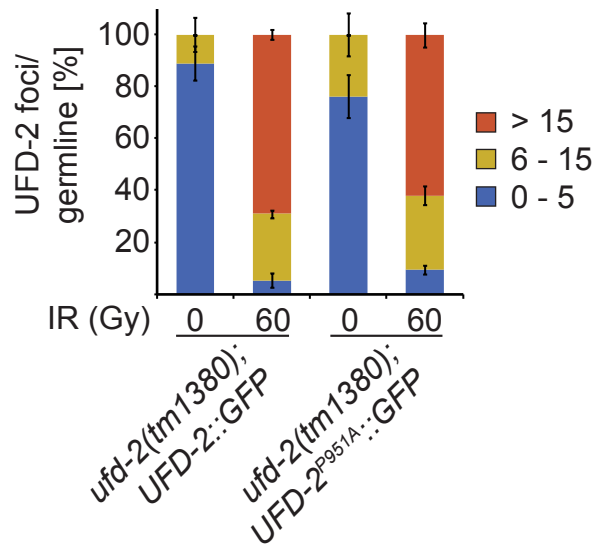
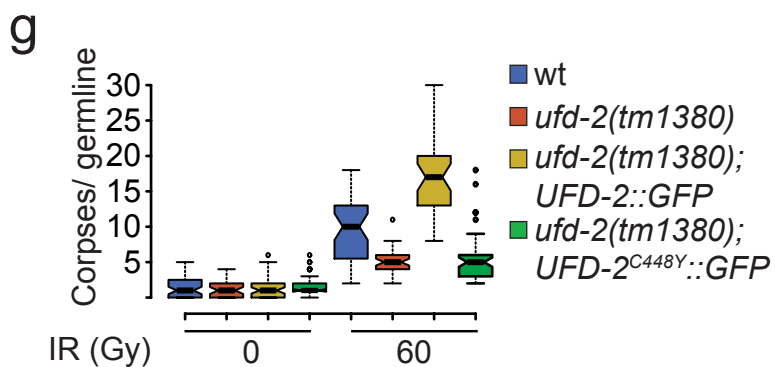
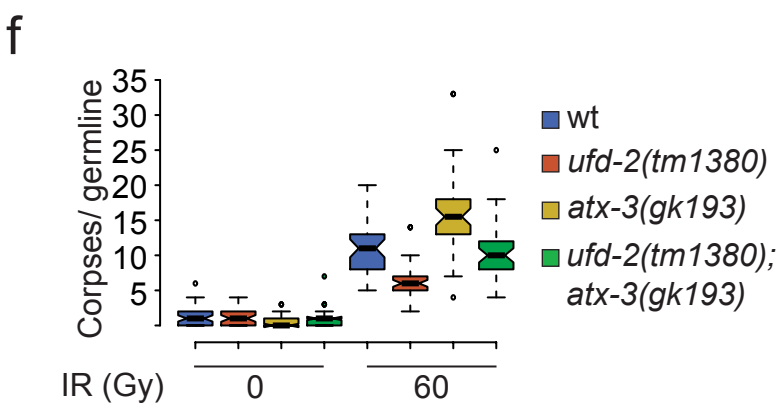
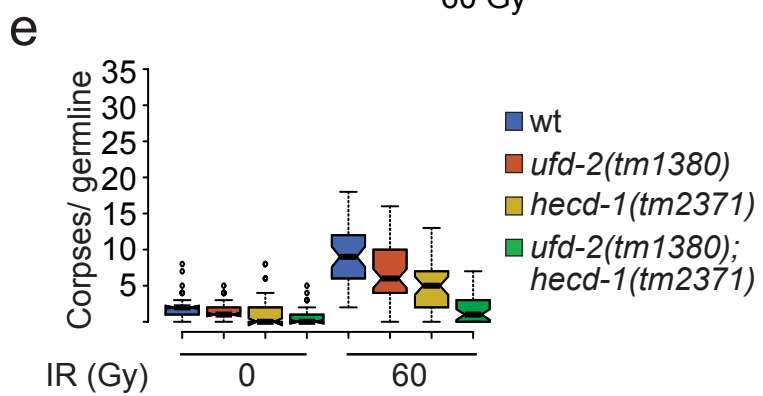
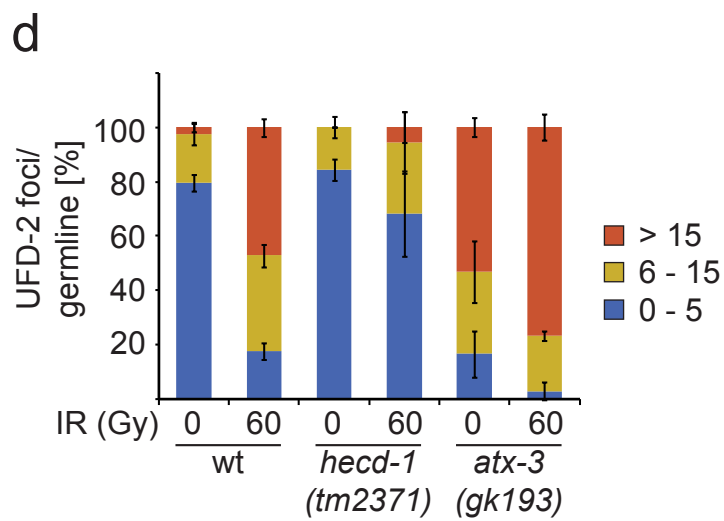
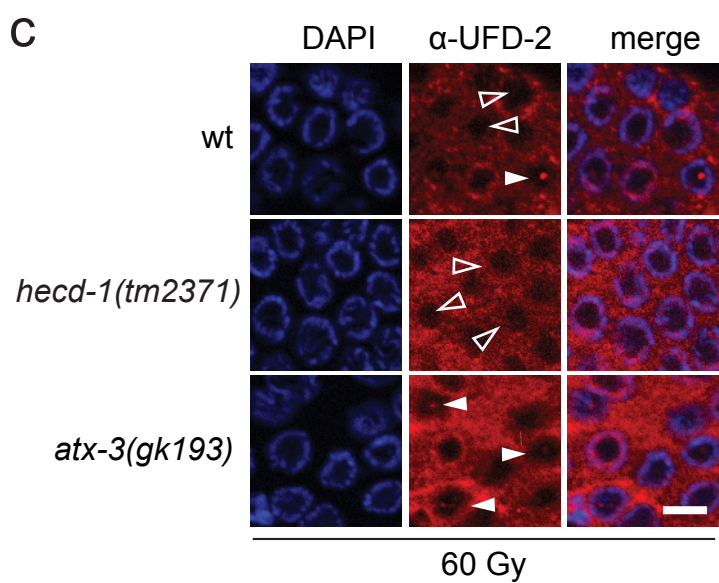
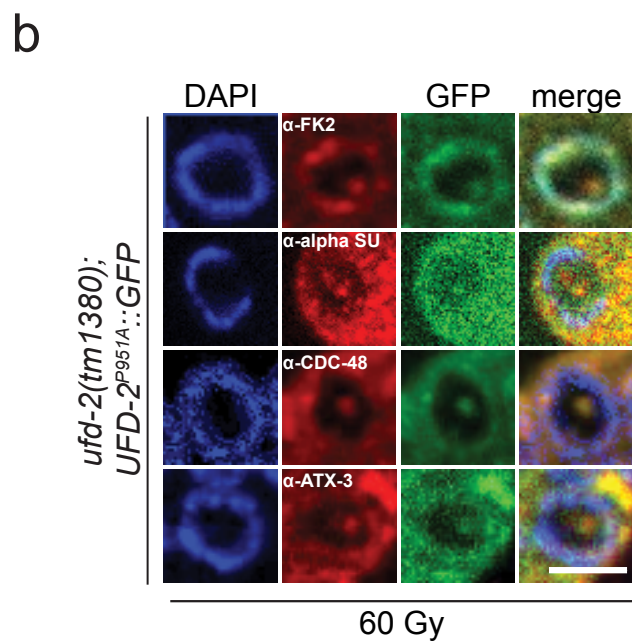
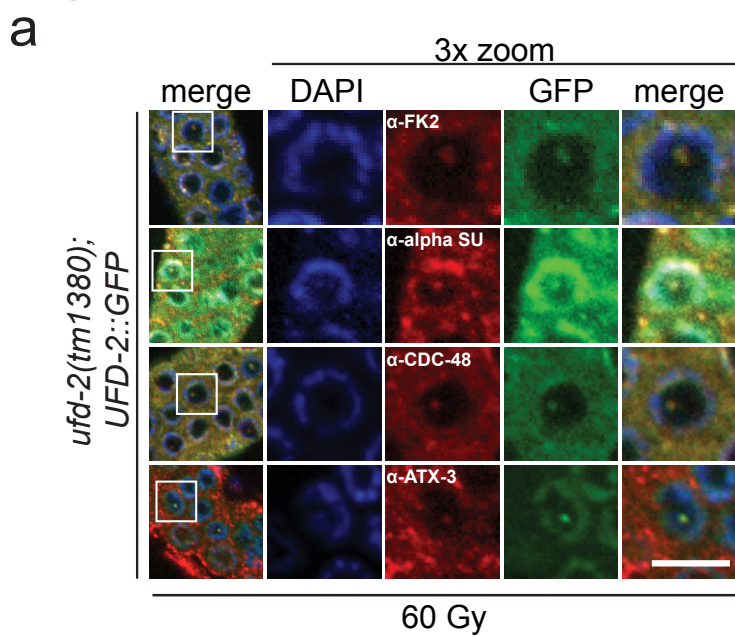


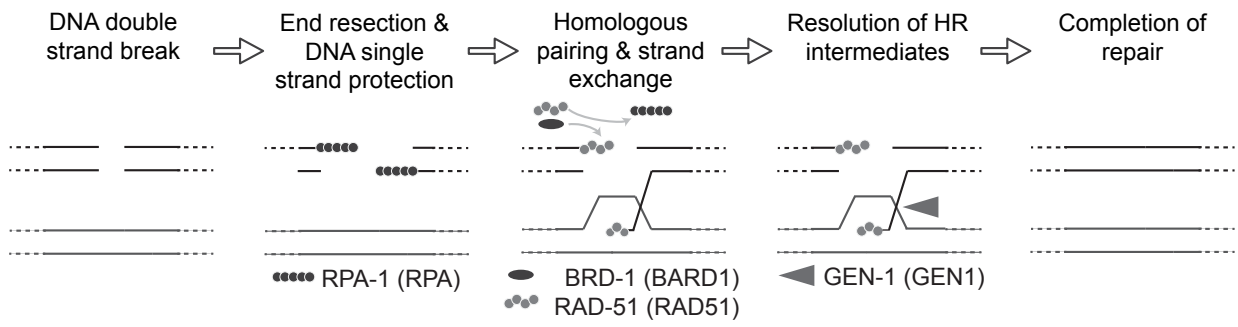
Figure 3



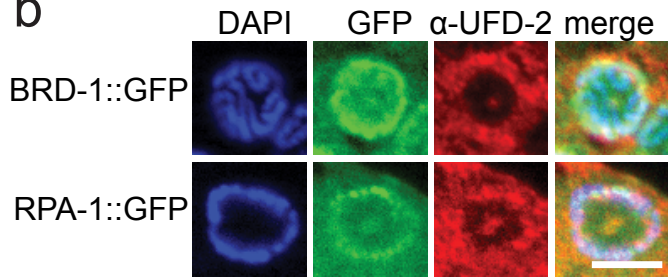


# Figure 4

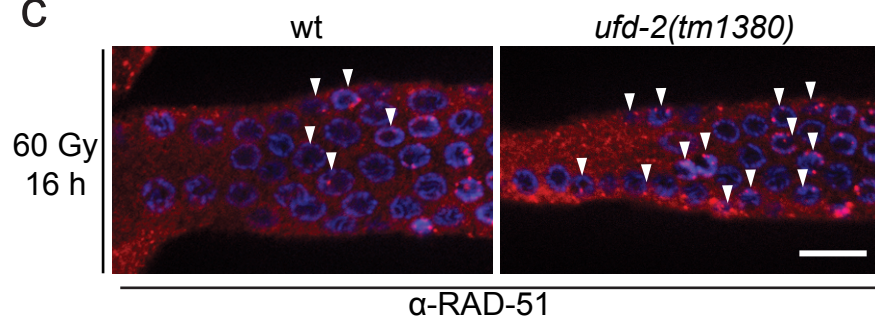
a



b



c



d

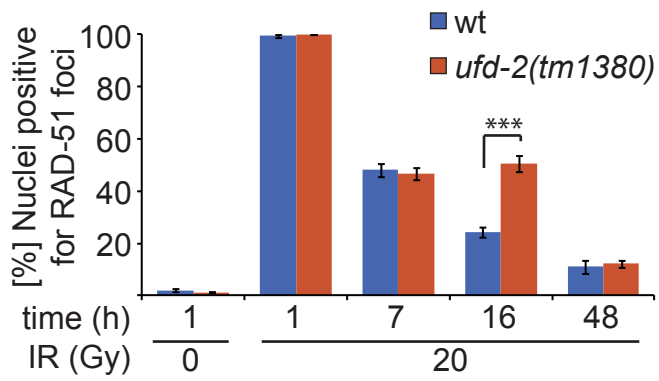


# Figure 5

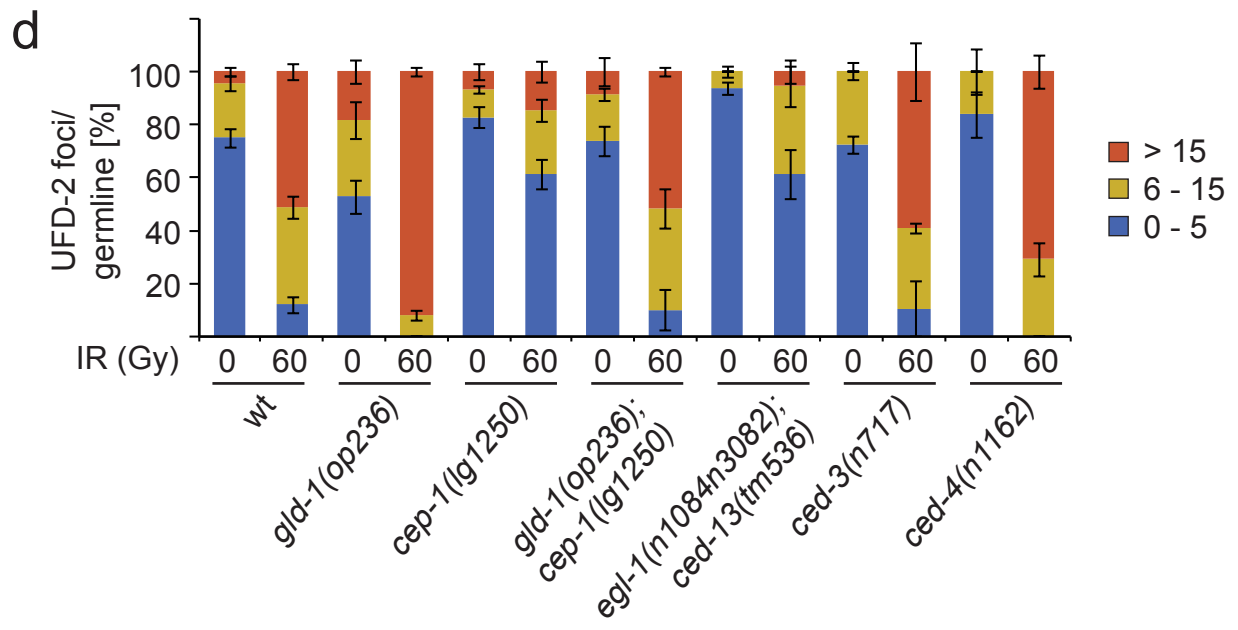
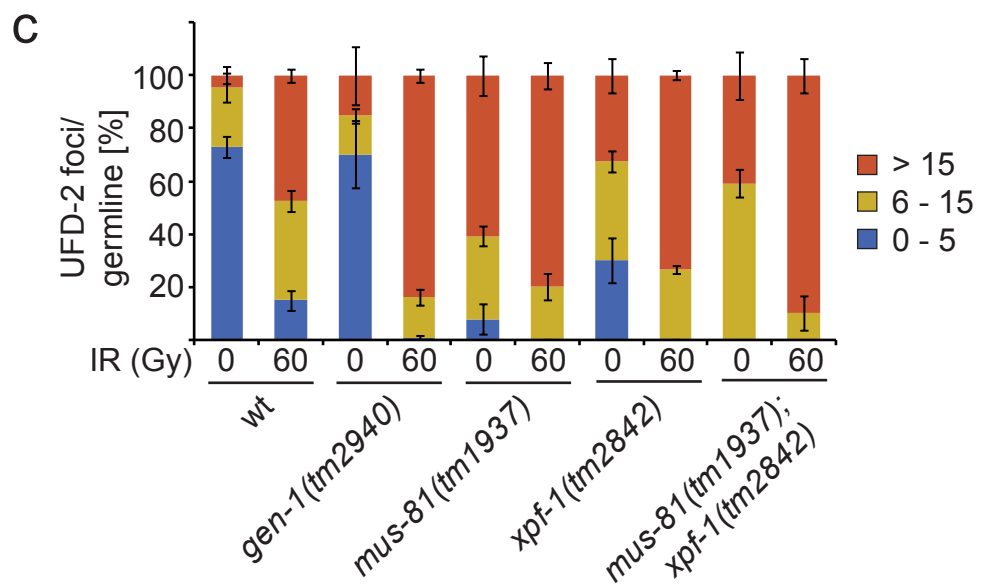
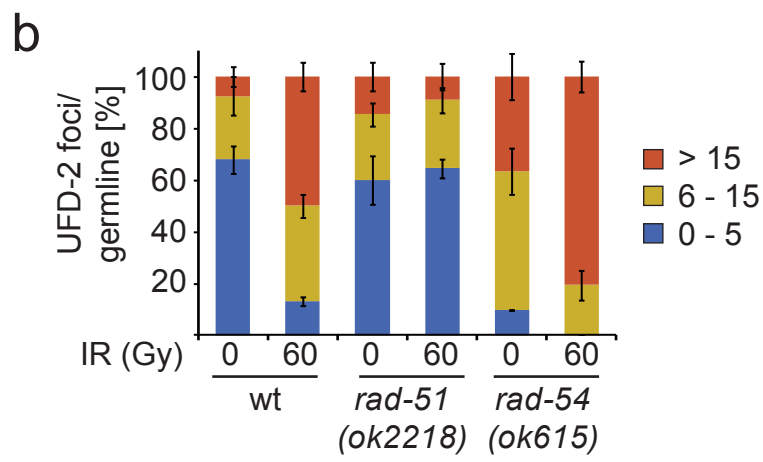
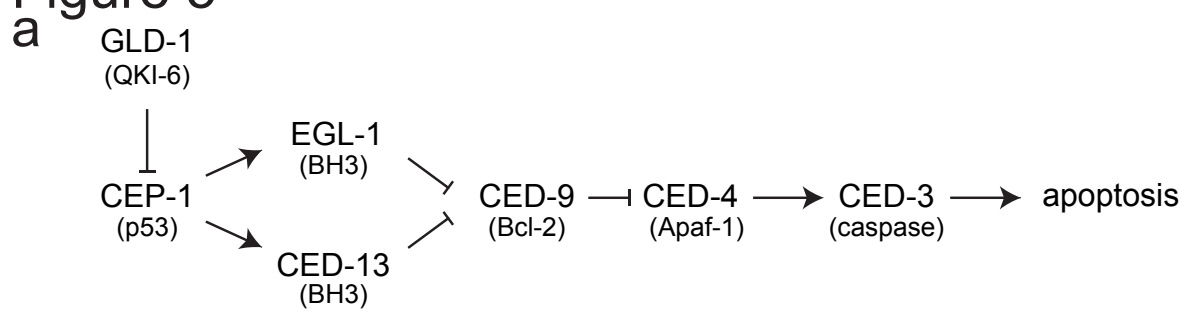


**Figure 6**

